Optical anisotropy of nanotube suspensions

Erik K. Hobbie[a)]
National Institute of Standards and Technology, Gaithersburg, Maryland 20899

(Received 16 January 2004; accepted 7 April 2004)

A semimacroscopic model of an optically anisotropic nanotube suspension is derived perturbatively from Maxwell's equations in a dielectric medium. We calculate leading-order expressions, valid in the dilute and semidilute limits, for the *intrinsic* and *form* contributions to the complex dielectric tensor in terms of the volume fraction, mean orientation, aspect ratio, optical anisotropy, and optical contrast of the nanotubes. The birefringence and dichroism are derived explicitly to leading order in fluctuations, and the connection with depolarized light scattering is established. The results are generalized to include tube deformation. © *2004 American Institute of Physics.*
[DOI: 10.1063/1.1760079]

I. INTRODUCTION

It is well known that flow can induce optical anisotropy in macromolecular fluids and colloidal suspensions in the form of birefringence and dichroism.[1,2] As first demonstrated by Peterlin and Stewart,[3] these effects separate naturally into two distinct parts; an *intrinsic* contribution arising from the orientation of optically anisotropic polymer segments or particles, and a *form* contribution arising from anisotropy in the segmental or density correlation function. The experimental techniques of flow birefringence and flow dichroism have proven to be powerful tools for studying the structural and dynamic properties of flowing polymer melts, polymer solutions, and anisotropic suspensions, which in turn has contributed to recent technological advances in the engineering and flow processing of complex fluids.

Recently, carbon nanotubes have emerged as novel materials with potential applications in a host of advanced technologies.[4] Nanocomposites engineered from polymers and carbon nanotubes, for example, offer the promise of plastic materials with enhanced structural, thermal, electronic, and optical properties. Efficient bulk processing of such composites will depend in part on a detailed understanding of the response of carbon nanotube suspensions and melts to flow. As colloidal particles, nanotubes are also somewhat unique and intriguing, in that they straddle the interface between semiflexible polymers and microscopic fibers. Given the significant optical contrast between carbon nanotubes and most typical polymers, it is reasonable to expect that such suspensions will exhibit reasonably strong optical anisotropy, making them well-suited to rheo-optical techniques.[5] Applied to such novel soft materials, the methods of flow birefringence and flow dichroism might offer new physical insight into both fundamental flow-structure relationships in anisotropic complex fluids, as well as fundamental information about the optical properties and optical anisotropy of the nanotubes themselves.

In this paper, we present a semimacroscopic calculation of the complex dielectric tensor of carbon nanotube suspensions and melts. The approach is reminiscent of the general theory of flow-induced optical anisotropy in dilute polymer solutions derived by Onuki and Doi,[6] and it expands on a previous treatment of depolarized light scattering from carbon nanotube suspensions.[5] We derive general expressions for both the *intrinsic* and *form* contributions to the dielectric tensor, and we derive leading-order expressions for the birefringence and dichroism. The connection to depolarized light scattering is established and the results are generalized to include tube deformation.

II. INTRINSIC CONTRIBUTION

For a quasistatic suspension of N optically anisotropic nanotubes in an optically isotropic solvent of dielectric constant ε_s illuminated by an incident electric field $\mathbf{E}(\mathbf{r},t)=\mathbf{E}_0 e^{i(\mathbf{k}\cdot\mathbf{r}-\omega t)}$, where $k^2=\varepsilon_s\omega^2/c^2$ and $\mathbf{k}$ points along the direction of propagation (see Fig. 1), the macroscopic dielectric tensor can be defined *via*

$$\mathbf{D}(\mathbf{r},t)=\tilde{\varepsilon}\cdot\mathbf{E}(\mathbf{r},t)=\tilde{\varepsilon}\cdot\mathbf{E}_0 e^{i(\mathbf{k}\cdot\mathbf{r}-\omega t)}, \tag{1}$$

where the tensor $\tilde{\varepsilon}=\Sigma_{\mu,\nu=1}^{3}\hat{\mathbf{x}}_\mu\varepsilon_{\mu\nu}\hat{\mathbf{x}}_\nu$ is homogeneous. If $\mathbf{r}$ locates a segment of a nanotube, $\hat{\mathbf{n}}(\mathbf{r})$, then the spatially varying amplitude of the displacement field induced at $\mathbf{r}$ is

$$\mathbf{D}(\mathbf{r})=\{\alpha_\parallel\hat{\mathbf{n}}(\mathbf{r})\hat{\mathbf{n}}(\mathbf{r})+\alpha_\perp[\mathbf{1}-\hat{\mathbf{n}}(\mathbf{r})\hat{\mathbf{n}}(\mathbf{r})]\}\cdot\mathbf{E}_0, \tag{2}$$

where the local *complex* dielectric constants $\alpha_\parallel$ and $\alpha_\perp$ arise from polarization and absorption along and normal to the local symmetry axis of the nanotube, respectively, and $\mathbf{1}$ is the identity tensor. The parameters $\alpha_\parallel$ and $\alpha_\perp$ appear in the formulas for the depolarized scattering of monochromatic light from nanotube suspensions.[5] Equation (2) defines a *local* dielectric tensor as

$$\tilde{\varepsilon}(\mathbf{r})=\alpha_\parallel\hat{\mathbf{n}}(\mathbf{r})\hat{\mathbf{n}}(\mathbf{r})+\alpha_\perp[\mathbf{1}-\hat{\mathbf{n}}(\mathbf{r})\hat{\mathbf{n}}(\mathbf{r})], \tag{3}$$

when $\mathbf{r}$ falls within a tube and $\tilde{\varepsilon}(\mathbf{r})=\varepsilon_s\mathbf{1}$ otherwise. Introducing the spatial average $\langle\tilde{\varepsilon}\rangle=V^{-1}\int d\mathbf{r}\tilde{\varepsilon}(\mathbf{r})$, where V is the sample volume, we obtain the *intrinsic* part of the dielectric tensor

$$\tilde{\varepsilon}_0=\langle\tilde{\varepsilon}\rangle=\phi[\alpha_\parallel\langle\hat{\mathbf{n}}_l\hat{\mathbf{n}}_l\rangle+\alpha_\perp(\mathbf{1}-\langle\hat{\mathbf{n}}_l\hat{\mathbf{n}}_l\rangle)]+(1-\phi)\varepsilon_s\mathbf{1}, \tag{4}$$

a)Electronic mail: erik.hobbie@nist.gov

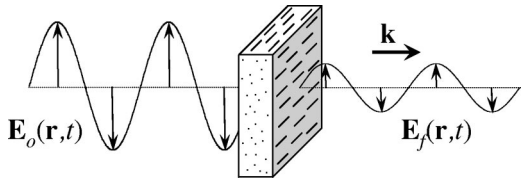

FIG. 1. A cartoon showing an aligned nanotube suspension. The suspending medium is of uniform dielectric constant ε_s. The incident field, $\mathbf{E}_0(\mathbf{r},t)$, is linearly polarized along the "slow" axis of the suspension. After transmission, the polarization is unchanged but the amplitude is attenuated by absorption. An incident field linearly polarized along the "fast" axis, or at 90° to the shown scenario, is altered in a similar manner. Light linearly polarized at an angle between these directions will also emerge attenuated, but with a polarization that is elliptical. We seek to calculate the effective dielectric tensor of the suspension.

where ϕ is the volume fraction and $\langle \hat{\mathbf{n}}_l \hat{\mathbf{n}}_l \rangle = N^{-1} \Sigma_l \hat{\mathbf{n}}_l \hat{\mathbf{n}}_l$. As in a previous derivation of the light-scattering amplitude,[5] we neglect contributions of linear and higher order in the difference between the end-to-end vector of the lth nanotube and its body director, $\hat{\mathbf{n}}_l$, which is equivalent to assuming that the tubes are nominally straight. The results will be generalized to include deformation.

III. SPATIAL FLUCTUATIONS

The earlier derivation gives just the leading-order part of the complex dielectric tensor. In general, there will be higher-order contributions arising from the spatial variations $\delta\tilde{\varepsilon}(\mathbf{r}) = \tilde{\varepsilon}(\mathbf{r}) - \langle \tilde{\varepsilon} \rangle$. Following Jackson's treatment of Rayleigh scattering,[7] we obtain these terms perturbatively from the vector wave equation for $\mathbf{D}$, which can be derived from Maxwell's equations in a dielectric medium. In the harmonic approximation in which all fields have a time dependence of the form $e^{i\omega t}$, this becomes an inhomogeneous vector Helmholtz equation

$$(\nabla^2 + k^2)\mathbf{D} = -\boldsymbol{\nabla}\times\boldsymbol{\nabla}\times(\mathbf{D} - \varepsilon_s \mathbf{E}). \tag{5}$$

Following Jackson,[7] the term in parenthesis on the right-hand side of Eq. (5) is written as $\delta\tilde{\varepsilon}(\mathbf{r})\cdot\mathbf{D}_0/\varepsilon_s$, where $\mathbf{D}_0 = \tilde{\varepsilon}_0 \cdot \mathbf{E}_0 e^{i\mathbf{k}\cdot\mathbf{r}}$. As in scattering theory, a formal solution is then obtained *via* successive iterations in terms of the Helmholtz Green's function

$$G(\mathbf{r},\mathbf{r}') = \frac{1}{4\pi}\frac{e^{ik|\mathbf{r}-\mathbf{r}'|}}{|\mathbf{r}-\mathbf{r}'|} = \frac{1}{(2\pi)^3}\int d\mathbf{q}\frac{e^{i\mathbf{q}\cdot(\mathbf{r}-\mathbf{r}')}}{q^2-(k+i\varsigma)^2}, \tag{6}$$

where the positive infinitesimal ς is needed to ensure causality in the displacement field, $\mathbf{D}(\mathbf{r},t)$.[6] The first-order correction is

$$\int d\mathbf{r}' G(\mathbf{r},\mathbf{r}')\nabla'\times\nabla'\times\delta\tilde{\varepsilon}(\mathbf{r}')\cdot\mathbf{D}_0'/\varepsilon_s = \int d\mathbf{r}'\,\delta\tilde{\varepsilon}(\mathbf{r}')\cdot(\mathbf{D}_0'/\varepsilon_s)\cdot[\boldsymbol{\nabla}'\boldsymbol{\nabla}' - (\nabla^2)'\mathbf{1}]G(\mathbf{r},\mathbf{r}'). \tag{7}$$

Multiplying by $e^{-i\mathbf{k}\cdot\mathbf{r}}$ to remove the harmonic spatial dependence and taking the spatial average, this term averages to zero,[8] and the first non-vanishing correction to $\mathbf{D}$ is thus second order in $\delta\tilde{\varepsilon}(\mathbf{r})$, being

$$\int d\mathbf{r}' G(\mathbf{r},\mathbf{r}')\boldsymbol{\nabla}'\times\boldsymbol{\nabla}'\times\frac{\delta\tilde{\varepsilon}(\mathbf{r}')}{\varepsilon_s}\cdot\int d\mathbf{r}'' G(\mathbf{r}',\mathbf{r}'')\boldsymbol{\nabla}''\times\boldsymbol{\nabla}'' \times\frac{\delta\tilde{\varepsilon}(\mathbf{r}'')}{\varepsilon_s}\cdot\mathbf{D}_0'', \tag{8}$$

which becomes

$$\int d\mathbf{r}'\frac{\delta\tilde{\varepsilon}(\mathbf{r}')}{\varepsilon_s}\cdot\int d\mathbf{r}'' e^{i\mathbf{k}\cdot\mathbf{r}''}\frac{\delta\tilde{\varepsilon}(\mathbf{r}'')}{\varepsilon_s}\cdot\tilde{\varepsilon}_0\cdot\mathbf{E}_0\cdot[\boldsymbol{\nabla}''\boldsymbol{\nabla}'' - (\nabla^2)''\mathbf{1}]G(\mathbf{r}',\mathbf{r}'')\cdot[\boldsymbol{\nabla}'\boldsymbol{\nabla}' - (\nabla^2)'\mathbf{1}]G(\mathbf{r},\mathbf{r}'). \tag{9}$$

Resolving the singularities in the Green's functions,[8] introducing their Fourier representation, multiplying by $e^{-i\mathbf{k}\cdot\mathbf{r}}$ and taking the spatial average, the correction to $\tilde{\varepsilon}_0$ is

$$\tilde{\varepsilon}_1 = \frac{\langle\delta\tilde{\varepsilon}^2\rangle}{\varepsilon_s^2}\cdot\tilde{\varepsilon}_0 + \frac{1}{(2\pi)^3}\int d\mathbf{q}\tilde{T}(\mathbf{k}-\mathbf{q})\cdot\tilde{\varepsilon}_0\cdot\left[\frac{-\mathbf{q}\mathbf{q}+k^2\mathbf{1}}{q^2-(k+i\varsigma)^2}\right], \tag{10}$$

where the tensor

$$\tilde{T}(\mathbf{q}) = \int d\mathbf{r} e^{-i\mathbf{q}\cdot\mathbf{r}}\langle\delta\tilde{\varepsilon}(\mathbf{r})\cdot\delta\tilde{\varepsilon}(0)\rangle/\varepsilon_s^2 \tag{11}$$

is related to the structure factor. Equation (10) is analogous to the expression derived by Onuki and Doi[6] and is quite general. As derived here, it contains two terms of $O(\delta\tilde{\varepsilon}^2/\varepsilon_s^2)$; a higher-order *intrinsic* correction arising purely from mean-square fluctuations and a leading-order *form* correction involving density correlations identical to that derived in Ref. 6. This result is somewhat intuitive, as one could envision particles lacking any spatial correlation that could still alter the polarization of incident light, with the physical scenario being optically anisotropic particles too small to visibly scatter. More quantitatively, for particles lacking any segmental correlation $\langle\delta\tilde{\varepsilon}(\mathbf{r})\cdot\delta\tilde{\varepsilon}(0)\rangle \approx \lim_{\xi\to 0}\langle\delta\tilde{\varepsilon}^2\rangle e^{-r^2/2\xi^2} \propto \lim_{\xi\to 0}\langle\delta\tilde{\varepsilon}^2\rangle\xi^3\delta(\mathbf{r})$, and the second term in Eq. (10) vanishes, implying that for such "formless" nanotubes the leading-order intrinsic correction to $\tilde{\varepsilon}_0$ is simply proportional to the mean-square deviation.[9] The full expression for the dielectric tensor is thus

$$\tilde{\varepsilon}\approx\left\{\mathbf{1} + \frac{\langle\delta\tilde{\varepsilon}^2\rangle}{\varepsilon_s^2} + \frac{1}{(2\pi)^3}\int d\mathbf{q}\tilde{T}(\mathbf{k}-\mathbf{q})\cdot\left[\frac{-\mathbf{q}\mathbf{q}+k^2\mathbf{1}}{q^2-(k+i\varsigma)^2}\right]\right\}\cdot\tilde{\varepsilon}_0 + \ldots, \tag{12}$$

where we have exploited that fact that $\tilde{\varepsilon}_0$ is symmetric.

IV. A USEFUL EXPANSION

Before deriving specific results applicable to limiting cases and scenarios of practical importance, it is useful to

recast the earlier results more explicitly in terms of the volume fraction of nanotubes. In this manner, the mean dielectric tensor is

$$\tilde{\varepsilon}_0=\varepsilon_s\mathbf{1}+\phi[(\alpha_\parallel-\alpha_\perp)\langle\hat{\mathbf{n}}_l\hat{\mathbf{n}}_l\rangle+(\alpha_\perp-\varepsilon_s)\mathbf{1}]\equiv\varepsilon_s\mathbf{1}+\phi\tilde{\beta}_0 \tag{13}$$

and the mean-square is

$$\langle\tilde{\varepsilon}^2\rangle=\varepsilon_s^2\mathbf{1}+\phi[(\alpha_\parallel^2-\alpha_\perp^2)\langle\hat{\mathbf{n}}_l\hat{\mathbf{n}}_l\rangle+(\alpha_\perp^2-\varepsilon_s^2)\mathbf{1}], \tag{14}$$

from which the mean-square deviation is $\langle\delta\tilde{\varepsilon}^2\rangle=\langle\tilde{\varepsilon}^2\rangle-\tilde{\varepsilon}_0^2=\phi\tilde{\beta}_1+\phi^2\tilde{\beta}_2$, where

$$\tilde{\beta}_1=(\alpha_\parallel-\alpha_\perp)(\alpha_\parallel+\alpha_\perp-2\varepsilon_s)\langle\hat{\mathbf{n}}_l\hat{\mathbf{n}}_l\rangle+(\alpha_\perp-\varepsilon_s)^2\mathbf{1} \tag{15}$$

and

$$\tilde{\beta}_2=(\alpha_\parallel-\alpha_\perp)^2\langle\hat{\mathbf{n}}_l\hat{\mathbf{n}}_l\rangle^2+2(\alpha_\parallel-\alpha_\perp)(\alpha_\perp-\varepsilon_s)\langle\hat{\mathbf{n}}_l\hat{\mathbf{n}}_l\rangle+(\alpha_\perp-\varepsilon_s)^2\mathbf{1}. \tag{16}$$

For the purpose of computing the two-point density correlation function, we can write

$$\delta\tilde{\varepsilon}(\mathbf{r})=(\alpha_\parallel-\alpha_\perp)\hat{\mathbf{n}}(\mathbf{r})\hat{\mathbf{n}}(\mathbf{r})+(\alpha_\perp-\varepsilon_s)\mathbf{1}, \tag{17}$$

when $\mathbf{r}$ locates an element of a nanotube, with $\delta\tilde{\varepsilon}(\mathbf{r})=0$ otherwise. Introducing the Fourier representation of $\delta\tilde{\varepsilon}(\mathbf{r})$, it is then easy to show that $\tilde{T}(\mathbf{q})=V^{-1}|\delta\tilde{\varepsilon}_\mathbf{q}|^2/\varepsilon_s^2$, where the *scattering amplitude tensor* is

$$\delta\tilde{\varepsilon}_\mathbf{q}\propto\sum_j[(\alpha_\parallel-\alpha_\perp)\hat{\mathbf{n}}_j\hat{\mathbf{n}}_j+(\alpha_\perp-\varepsilon_s)\mathbf{1}]e^{-i\mathbf{q}\cdot\mathbf{r}_j}, \tag{18}$$

the index j running over all of the scattering elements of the system. The connection to depolarized light scattering is now apparent,[10] with each of the four structure factors[5] being the square modulus of the corresponding Cartesian projection of the tensor $\delta\tilde{\varepsilon}_\mathbf{q}$. Following the analysis in Ref. 5, we decompose this tensor into inter and intratube contributions to obtain

$$\delta\tilde{\varepsilon}_\mathbf{q}=\sum_{l=1}^N[(\alpha_\parallel-\alpha_\perp)\hat{\mathbf{n}}_l\hat{\mathbf{n}}_l+(\alpha_\perp-\varepsilon_s)\mathbf{1}]e^{-i\mathbf{q}\cdot\mathbf{r}_l}\times\int_{v_l}d\mathbf{r}'e^{-i\mathbf{q}\cdot\mathbf{r}'}, \tag{19}$$

where $\hat{\mathbf{n}}_l$, $\mathbf{r}_l$, and v_l are the director, center of mass, and volume of the lth nanotube, respectively, and $\mathbf{r}'$ locates the volume element $d\mathbf{r}'$ with respect to the center of mass, $\mathbf{r}_l$. For reasonably monodisperse nanotubes with random centroids, $\mathbf{r}_l$, we obtain

$$\tilde{T}(\mathbf{q})\approx\phi\tilde{\beta}_1\langle|f_l(\mathbf{q})|^2\rangle/v\varepsilon_s^2, \tag{20}$$

where v is the average volume and

$$f_l(\mathbf{q})=\int_{v_l}d\mathbf{r}e^{-i\mathbf{q}\cdot\mathbf{r}} \tag{21}$$

is a *form amplitude* that depends on the shape and orientation of the lth tube. The earlier expression for $\tilde{T}(\mathbf{q})$ will be precise in the dilute and semidilute limits, where the distribution of centroids is essentially random, and when there is limited polydispersity. Otherwise it will be an approximation. The validity of Eq. (20) also depends on the decoupling

$$\sum_{l=1}^N\hat{\mathbf{n}}_l\hat{\mathbf{n}}_l|f_l(\mathbf{q})|^2\approx\langle\hat{\mathbf{n}}_l\hat{\mathbf{n}}_l\rangle\sum_{l=1}^N|f_l(\mathbf{q})|^2+\ldots, \tag{22}$$

which is reasonable for some director distributions, but will involve higher-order corrections that we neglect here but consider at the end of the paper. The full expression for $\tilde{\varepsilon}$, otherwise exact to $O(\delta\tilde{\varepsilon}^2)$, is thus

$$\tilde{\varepsilon}\approx\varepsilon_s\mathbf{1}+\phi\left\{\tilde{\beta}_0+\frac{\tilde{\beta}_1}{\varepsilon_s}\cdot[\mathbf{1}+\tilde{\mathrm{I}}(\mathbf{k})]\right\}+\phi^2\left\{\frac{\tilde{\beta}_2}{\varepsilon_s}+\frac{\tilde{\beta}_1\cdot\tilde{\beta}_0}{\varepsilon_s^2}\cdot[\mathbf{1}+\tilde{\mathrm{I}}(\mathbf{k})]\right\}+\phi^3\left\{\frac{\tilde{\beta}_2\cdot\tilde{\beta}_0}{\varepsilon_s^2}+\ldots\right\}+\ldots, \tag{23}$$

where

$$\tilde{\mathrm{I}}(\mathbf{k})=\frac{1}{(2\pi)^3v}\int d\mathbf{q}\langle|f_l(\mathbf{k}-\mathbf{q})|^2\rangle\left[\frac{-\mathbf{qq}+k^2\mathbf{1}}{q^2-(k+i\varsigma)^2}\right]. \tag{24}$$

There are terms of relevant order in ϕ that we have neglected in Eq. (23), but these will be of higher order in the optical anisotropy and contrast, being of $O(\delta\tilde{\varepsilon}^4)$ or higher. In the long wavelength ($k\to0$) limit, Eq. (24) simplifies to

$$\tilde{\mathrm{I}}_0=-\frac{1}{(2\pi)^3v}\int d\mathbf{q}\langle|f_l(\mathbf{q})|^2\rangle\hat{\mathbf{q}}\hat{\mathbf{q}}. \tag{25}$$

In this approximation, the imaginary part of Eq. (24)—which arises from the pole structure of the integrand and, in nonabsorbing materials, gives rise to turbidity and what is known as *form dichroism*[6,11] in anisotropic systems—vanishes. Physically, this is equivalent to assuming that absorption dominates scattering, where the latter scales as k^4.[7] Depending on the size of the tubes, this approximation will be reasonable for dilute to semidilute carbon nanotube suspensions. As evidence for this, we measured the absolute turbidity ($\lambda=632.8$ nm) due to scattering in nonabsorbing spherical colloidal suspensions prepared at a fixed volume fraction of $\phi_0\approx10^{-3}$. For aqueous latex suspensions of diameter $d=11$ μm, 230, and 40 nm, the measured turbidity is 0.22, 0.59, and 0.12 mm^{-1}, respectively, the turbidity of the empty quartz cell being 0.07 mm^{-1}. For all three of these suspensions, $\Delta n/n_s\approx(1.6-1.33)/1.33\approx0.2$, and the 2-mm-thick samples were visually transparent. In contrast, a suspension of multiwalled carbon nanotubes (MWNTs) dispersed in toluene at the same volume fraction (with a mean tube length of $L=10$ μm and a mean tube diameter of $2a=50$ nm) exhibits an attenuation of 0.95 mm^{-1}. In the 2-mm-thick quartz cell, the MWNT-toluene suspension had a black hue but was also visually transparent. The index of refraction of toluene is of order 1.5 and previous reflectivity measurements[5] suggest that the approximate modulus of the complex MWNT refractive index is of order 1.6. Comparing the measured turbidity of the MWNT suspension with that of the 11 μm and 40 nm spherical latex suspensions—which span the same physical dimensions and have roughly $3\times$ the optical contrast—we see that absorption accounts for *at least* 85% of attenuation in the MWNT suspension, consistent with the earlier approximation. At this volume fraction, we

note that $(4/\pi)\phi_0(L/d)^2 \approx 50$ and $(4/\pi)\phi_0(L/d) \approx 0.25$, with the MWNT suspension being well into the semidilute regime.

V. LIMITING CASES

By dispersing the nanotubes in a viscoelastic polymer melt or solution, flow can be used to orient the tubes, where the direction and extent of orientation depend on the type of flow, the tube aspect ratio,[12] the fluid elasticity,[13] and, for semidilute suspensions, hydrodynamic interactions.[14,15] For dilute and semidilute suspensions in purely viscous fluids under simple steady shear flow, the distribution of fiber orientations is broadly peaked along a direction very close to the flow axis.[12–15] In viscoelastic fluids under shear, the observed orientation is somewhat more complicated. For dilute suspensions of fibers in weakly elastic fluids, or at a small Deborah number (defined as the product of the shear rate and a linear-viscoelastic relaxation time), the steady-state orientation is along the direction of vorticity, perpendicular to the plane defined by the flow and velocity-gradient directions.[16] At higher concentrations in such fluids, however, both flow and vorticity alignment have been reported.[13,16] In contrast, for dilute and semidilute suspensions in highly elastic fluids, or at a high Deborah number, strong flow alignment is observed,[13,17] while for dilute suspensions in fluids of intermediate elasticity, the fibers orient at well-defined angles in the flow-vorticity plane.[17] Although the situation is complex, the most striking and relevant feature is a deviation from the stress-optical rule in its usual form, which states that the direction of greatest optical anisotropy is along the direction of principle strain, which for shear flow is at 45° in the flow-gradient plane.[1,6,18] In contrast, at least for nanotubes that can be modeled as long stiff fibers, we would expect that in many cases the dielectric tensor will be diagonal in the orthogonal coordinate system defined by the flow field. The dynamic nature of the tube orbits and, at low Peclet number, thermal fluctuations will both influence the steady-state distribution.

We can thus cover a broad range of physically relevant situations by considering the three scenarios in Fig. 2. An isotropic distribution [Fig. 2(a)] is trivial, since there is no anisotropy in Eq. (23), and the idealized scenario in Fig. 2(b) can be viewed as a limiting case of the general situation depicted in Fig. 2(c) in which the width of the angular distribution tends to zero, so we focus on the distribution in Fig. 2(c). The form amplitude of a tube of length L_l and radius a_l, centered at the origin with its director $\hat{\mathbf{n}}_l$ pointing along the x axis, is

$$f_l(\mathbf{q}) = 2v_l \frac{\sin(L_l q_x/2)}{(L_l q_x/2)} \frac{J_1(a_l q_\perp)}{a_l q_\perp}, \tag{26}$$

where $J_1(y)$ is the Bessel function of the first kind of order 1, $\mathbf{q}_\perp = q_x\hat{\mathbf{x}} + q_y\hat{\mathbf{y}}$, and $v_l = \pi a_l^2 L_l$. This expression [Eq. (26)] can be transformed to the general situation in which the tube axis makes an angle θ_l with the x axis by a rotation, which leads to the substitutions

$$q_x \to q_x \cos\theta_l + \mathbf{q}_\perp \cdot \hat{\mathbf{e}}_\perp^{(2)} \sin\theta_l \tag{27}$$

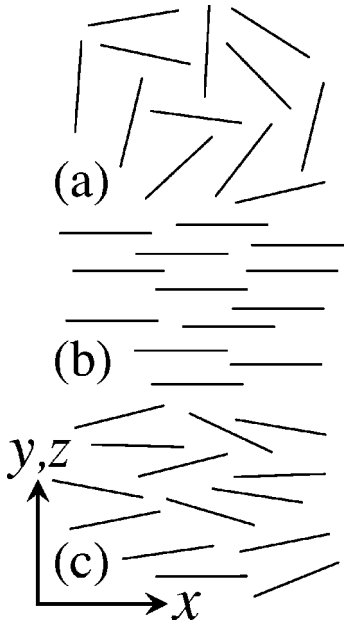

FIG. 2. A cartoon showing three different scenarios of tube orientation. The x axis indicates the direction of flow, and in each case the director distribution is assumed to be symmetric around the y and z axes. An isotropic suspension (a) exhibits no anisotropy, while a perfectly aligned suspension (b) exhibits anisotropy reflecting that of the individual nanotubes in the limit of infinite dilution. The scenario in (c) models a broad number of physically relevant situations. For suspensions under shear flow, tubes will be in periodic Jeffery orbits around the z axis, and the director distribution function can be computed as either a temporal average over a moving ensemble containing the same tubes or as a temporal average over a fixed spatial region, with each ''snap-shot'' of the ensemble containing a new set of tubes.

and

$$q_\perp^2 \to [\mathbf{q}_\perp \cdot \hat{\mathbf{e}}_\perp^{(1)}]^2 + [\mathbf{q}_\perp \cdot \hat{\mathbf{e}}_\perp^{(2)} \cos\theta_l - q_x \sin\theta_l]^2, \tag{28}$$

where $\hat{\mathbf{e}}_\perp^{(1)} = \hat{\mathbf{n}}_l \times \hat{\mathbf{x}}/|\hat{\mathbf{n}}_l \times \hat{\mathbf{x}}|$ and $\hat{\mathbf{e}}_\perp^{(2)} = \hat{\mathbf{x}} \times \hat{\mathbf{e}}_\perp^{(1)}$. To proceed further, we note that for ease of computation (and to a reasonably good approximation, particularly in the presence of polydispersity) we can model the square of the functions appearing in Eq. (26) with Gaussians as

$$\frac{\sin^2(x)}{x^2} \frac{J_1^2(y)}{y^2} \approx \frac{1}{4} \exp\left(-\frac{x^2}{3} - \frac{y^2}{4} \right) + \ldots, \tag{29}$$

with $x = L_l q_x/2$ and $y = a_l q_\perp$, from which we obtain

$$\begin{aligned} \langle |f_l(\mathbf{q})|^2 \rangle &\approx v^2 \left\{ 1 - \frac{q_x^2}{4} \left[\frac{L^2 \psi}{3} + a^2(1-\psi) \right] \right. \\ &\quad \left. - \frac{q_\perp^2}{8} \left[a^2(1+\psi) + \frac{L^2}{3}(1-\psi) \right] + \ldots \right\} \\ &\approx v^2 \exp[-(\xi_\parallel q_x)^2 - (\xi_\perp q_\perp)^2], \end{aligned} \tag{30}$$

where we have introduced $\psi = \langle \cos^2\theta \rangle$—equal to 1 for perfect alignment and 1/3 for a random distribution—and we have approximated the truncated series with a Gaussian. The correlation lengths appearing in Eq. (30) are

$$\xi_\parallel^2 = [L^2\psi/3 + a^2(1-\psi)]/4 \tag{31}$$

and

$$\xi_\perp^2 = [a^2(1+\psi) + L^2(1-\psi)/3]/8. \tag{32}$$

The integrals involved in evaluating Eq. (25) are nontrivial, although by symmetry $\tilde{\mathrm{I}}_0$ is diagonal. We make one more simplifying approximation by exploiting the fact that for reasonably well-aligned tubes of sufficiently high aspect ratio, we have $\xi_\parallel \gg \xi_\perp$, in which case $(\tilde{\mathrm{I}}_0)_{xx} \approx 0$ and

$$\tilde{\mathrm{I}}_0 \approx -(16\pi^{1/2})^{-1}(L/\xi_\parallel)(a/\xi_\perp)^2(\hat{\mathbf{y}}\hat{\mathbf{y}} + \hat{\mathbf{z}}\hat{\mathbf{z}}) + \ldots. \tag{33}$$

Finally, we note that for the ellipsoidal model we are considering

$$\langle \hat{\mathbf{n}}_l \hat{\mathbf{n}}_l \rangle = \psi \hat{\mathbf{x}}\hat{\mathbf{x}} + \tfrac{1}{2}(1-\psi)(\hat{\mathbf{y}}\hat{\mathbf{y}} + \hat{\mathbf{z}}\hat{\mathbf{z}}). \tag{34}$$

All of the elements of the dielectric tensor are now cast explicitly in terms of ϕ, ψ, L, a, $\alpha_\perp$, $\alpha_\parallel$, and ε_s.

VI. BIREFRINGENCE AND DICHROISM

Because the parameters $\alpha_\perp$ and $\alpha_\parallel$ are complex, the dielectric tensor will contain real and imaginary parts. In the orthogonal coordinates defined by the principal axes of $\tilde{\varepsilon}$, one then has $\tilde{\varepsilon}_{\mu\nu} = e_\nu \delta_{\mu\nu}$, where e_1, e_2, and e_3 are the three complex eigenvalues of $\tilde{\varepsilon}$. The three complex refractive indices are $n_\nu = n'_\nu + i n''_\nu = \sqrt{e_\nu}$, with the birefringence and dichroism defined as the difference between the largest and smallest values of the real and imaginary parts, respectively. In contrast to polymer solutions, the intrinsic dichroism of a carbon nanotube suspension will be significant, reflecting the imaginary component of the polarizability, which gives rise to absorption. The intensity of light polarized along the direction ν will be attenuated *via* $\exp(-4\pi n''_\nu d/\lambda)$, where λ is the wavelength in air and d the propagation distance. Splitting the νth eigenvalue of $\tilde{\varepsilon}$ into real and imaginary parts as $e_\nu = e'_\nu + i e''_\nu$, one obtains the exact relations

$$n'_\nu = \left\{ \frac{e'_\nu + [(e'_\nu)^2 + (e''_\nu)^2]^{1/2}}{2} \right\}^{1/2} \tag{35}$$

and

$$n''_\nu = \left\{ \frac{-e'_\nu + [(e'_\nu)^2 + (e''_\nu)^2]^{1/2}}{2} \right\}^{1/2}, \tag{36}$$

where $\nu = 1, 2, 3$. For the model derived here, $e_\parallel = (\tilde{\varepsilon})_{xx}$ and $e_\perp = (\tilde{\varepsilon})_{yy} = (\tilde{\varepsilon})_{zz}$, with the birefringence and dichroism $\Delta n' = n'_\parallel - n'_\perp$ and $\Delta n'' = n''_\parallel - n''_\perp$, respectively.

Comparison with experiment might require a numerical computation of the earlier quantities, but for the sake of illustration we explicitly consider only the leading-order contribution here, noting that without some type of small-contrast approximation, the general expressions become quite involved. Then

$$n_\parallel = \sqrt{e_\parallel} \approx \varepsilon_s + \tfrac{1}{2}\phi\psi[(\alpha'_\parallel - \alpha'_\perp) + i(\alpha''_\parallel - \alpha''_\perp)] + \ldots \tag{37}$$

and

$$n_\perp = \sqrt{e_\perp} \approx \varepsilon_s + \tfrac{1}{4}\phi(1-\psi)[(\alpha'_\parallel - \alpha'_\perp) + i(\alpha''_\parallel - \alpha''_\perp)] + \ldots, \tag{38}$$

from which

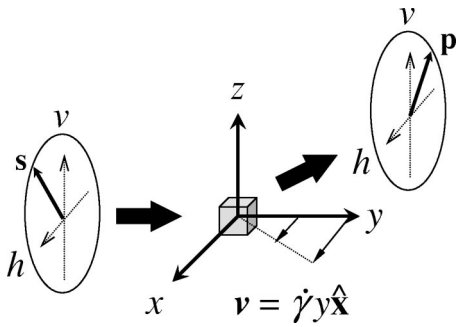

FIG. 3. The geometry of depolarized flow light scattering, where **s** is the polarization of the incident beam and **p** is the polarization of the analyzer. For simple shear, the flow direction is along the x axis, the gradient direction is along the y axis, and the vorticity direction is along the z axis. In previous publications (see Refs. 5 and 13), the x direction is referred to as h and the z direction is referred to as v. We consider scattering in the x–z plane, with the four structure factors given by the four permutations of **s** and **p**. The shear rate is $\dot{\gamma} = \partial v_x / \partial y$.

$$\Delta n' \approx \tfrac{3}{4}(\alpha'_\parallel - \alpha'_\perp)\phi(\psi - \tfrac{1}{3}) + \ldots \tag{39}$$

and

$$\Delta n'' \approx \tfrac{3}{4}(\alpha''_\parallel - \alpha''_\perp)\phi(\psi - \tfrac{1}{3}) + \ldots. \tag{40}$$

The quantity $(3/2)(\psi - 1/3)$ is a *nematic* order parameter, being zero for a random distribution and 1 for perfect alignment. Equations (39) and (40) will only be rigorously correct in the limit of small volume fraction, and for larger ϕ one might need higher-order corrections, evaluating $n_\parallel$ and $n_\perp$ explicitly in terms of the real and imaginary parts of the diagonal elements of the dielectric tensor. In principle, however, a direct measure of the optical anisotropy of nanotubes can be determined from rheo-optical data if the order parameter can be measured independently. Conversely, if the optical anisotropy of the tubes is known, the order parameter can be determined from a measurement of either the birefringence or the dichrosim. Analogous versions of Eqs. (39) and (40) are derived *via* alternate approaches by Fuller[1] and Eq. (39) is recently derived in the context of rod-like particle suspensions by Lenstra, Dogic, and Dhont.[19]

VII. CONNECTION TO LIGHT SCATTERING

If the tubes have no optical anisotropy, then the light-scattering intensity is simply proportional to $\langle |f_l(\mathbf{q})|^2 \rangle$. Otherwise, for a given scattering geometry (Fig. 3) there are four structure factors

$$S_{\mu\nu}(\mathbf{q}) \propto |\hat{\mathbf{x}}_\mu \cdot \delta\tilde{\varepsilon}_\mathbf{q} \cdot \hat{\mathbf{x}}_\nu|^2 = \left| \sum_l [(\alpha_\parallel - \alpha_\perp)\hat{\mathbf{x}}_\mu \cdot \hat{\mathbf{n}}_l \hat{\mathbf{n}}_l \cdot \hat{\mathbf{x}}_\nu + (\alpha_\perp - \varepsilon_s)\delta_{\mu\nu}] f_l(\mathbf{q}) e^{-i\mathbf{q}\cdot\mathbf{r}_l} \right|^2. \tag{41}$$

As in Sec. IV, for a random distribution of nanotube centroids this reduces to

$$S_{\mu\nu}(\mathbf{q}) \propto \sum_l \left| (\alpha_\parallel - \alpha_\perp)\hat{\mathbf{x}}_\mu \cdot \hat{\mathbf{n}}_l \hat{\mathbf{n}}_l \cdot \hat{\mathbf{x}}_\nu + (\alpha_\perp - \varepsilon_s)\delta_{\mu\nu} \right|^2 |f_l(\mathbf{q})|^2. \tag{42}$$

In the decoupling approximation Eq. (22), the four structure factors have the same anisotropy. Although this approximation might be appropriate at the level of computing the form birefringence and dichroism—particularly in light of the strong intrinsic terms—simple consideration of $S_{\mu\nu}(\mathbf{q})$ shows that it is not appropriate for scattering; $\tilde{\varepsilon}$ will always be isotropic for random distributions but $S_{\mu\nu}(\mathbf{q})$ is by definition *anisotropic*. We thus require a more exact coupling scheme, and the following approach can be used to refine Eq. (20). Written out explicitly, the three independent structure factors in the $x-z$ plane are

$$S_{xx}(\mathbf{q}) = V^{-1}\varepsilon_s^{-2}\sum_l \left[|\delta_1|^2 + 2\,\mathrm{Re}(\delta_1^*\delta_2)\cos^2\theta_l + |\delta_2|^2\cos^4\theta_l \right] |f_l(\mathbf{q})|^2, \tag{43}$$

$$S_{zz}(\mathbf{q}) = V^{-1}\varepsilon_s^{-2}\sum_l \left[|\delta_1|^2 + 2\,\mathrm{Re}(\delta_1^*\delta_2)\sin^2\theta_l\cos^2\varphi_l + |\delta_2|^2\sin^4\theta_l\cos^4\varphi_l \right] |f_l(\mathbf{q})|^2, \tag{44}$$

and

$$S_{xz}(\mathbf{q}) = S_{zx}(\mathbf{q}) = V^{-1}\varepsilon_s^{-2}|\delta_2|^2\sum_l \cos^2\theta_l \sin^2\theta_l \cos^2\varphi_l |f_l(\mathbf{q})|^2, \tag{45}$$

where $\delta_1 = \alpha_\perp - \varepsilon_s$, $\delta_2 = \alpha_\parallel - \alpha_\perp$, and $f_l(\mathbf{q})$ is given by Eq. (26) with the substitutions (27) and (28). Evaluation of Eqs. (43)–(45) is done numerically for a given orientational distribution, $p(\theta)$.

Figure 4 shows the computed depolarized structure factors for an isotropic distribution of nanotubes in the Gaussian approximation [Eq. (29)] with $L = 10\ \mu$m, $a = 25$ nm, $|\delta_1|^2/\varepsilon_s^2 = 0.3$, $|\delta_2|^2/\varepsilon_s^2 = 0.28$, and $2\,\mathrm{Re}(\delta_1^*\delta_2)/\varepsilon_s^2 = 0.58$. As an approximation, $\alpha_\perp$ and $\alpha_\parallel$ are assumed real. Measurements on aligned *metallic* single-walled carbon nanotubes (SWNTs) suggest that there is no absorption normal to the tube axis, with strong absorption parallel to the tube axis.[20] For MWNTs, which typically have a larger number of defects in their graphitic structure, this absorption anisotropy will be present but less pronounced, and we neglect it here as a first approximation. A comparison between experiment and theory that accounts for absorption and incorporates a variety of rheo-optical measurements will be reported elsewhere. The calculations reproduce the distinctive features of measured depolarized light-scattering patterns under comparable conditions (Fig. 5), and a quantitative study of the effect of varying anisotropy is shown in Fig. 6. Assuming $\varepsilon_s \approx 1.5$, $\delta_2/\delta_1 \approx 1.83$ implies $\alpha_\parallel/\alpha_\perp \approx 3$, somewhat higher than the upper limit of scattering anisotropy measured for aligned SWNT bundles.[21] Increasing δ_1 with respect to δ_2 (or, equivalently, decreasing $\alpha_\parallel/\alpha_\perp$) gives good agreement between the MWNT data and theory, with the data suggesting

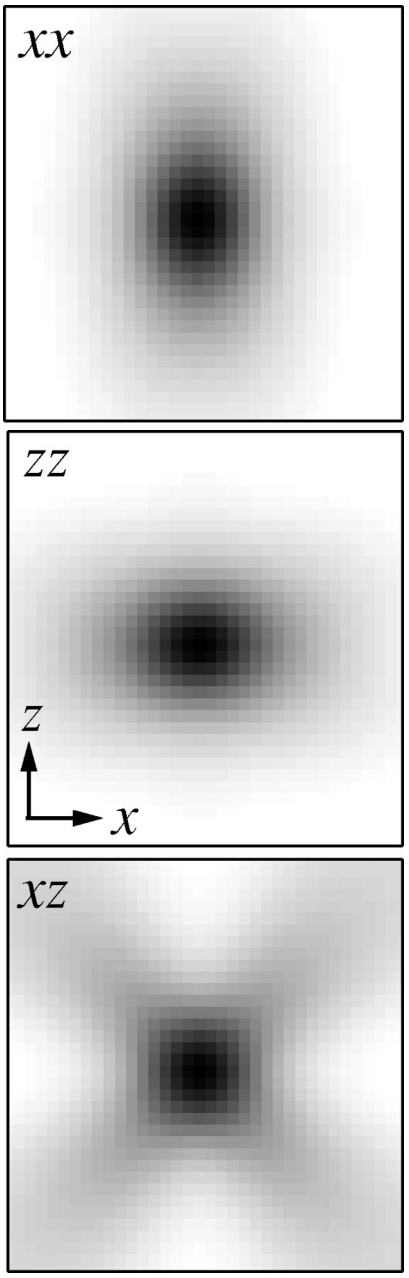

FIG. 4. The numerically computed structure factors for an isotropic distribution of nanotubes in the Gaussian approximation [Eq. (29)], with $L = 10\ \mu$m, $a = 25$ nm, $|\delta_1|^2/\varepsilon_s^2 = 0.3$, $|\delta_2|^2/\varepsilon_s^2 = 0.28$, and $2\,\mathrm{Re}[\delta_1^*\delta_2]/\varepsilon_s^2 = 0.58$. The width of each scattering pattern is $3.5\ \mu\mathrm{m}^{-1}$. These parameters are chosen to reflect the physical dimensions of the MWNTs used for scattering and microscopy measurements (Fig. 5), with the optical anisotropy adjusted to obtain agreement with the data in Fig. 5.

$\alpha_\parallel/\alpha_\perp \approx 1.4$, somewhat lower than the lower limit of scattering anisotropy measured for aligned SWNT bundles.[21] The approximate q^{-1} scattering envelope in Fig. 6 arises from the tube-like structure of the MWNTs. For a semiflexible chain of arbitrary orientation, the radial density of scattering elements is $n(r) \propto r^D$, where $D \geq 1$ is the fractal dimension of the chain. The radial distribution function is thus $g(r) \propto r^{1-d}\partial n/\partial r \propto r^{D-d}$, from which $S(q) \propto q^{-D}$.

VIII. TUBE DEFORMATION

The micrographs in Fig. 5 suggest that the nanotubes are not ideally straight. Tube deformation can arise from a vari-

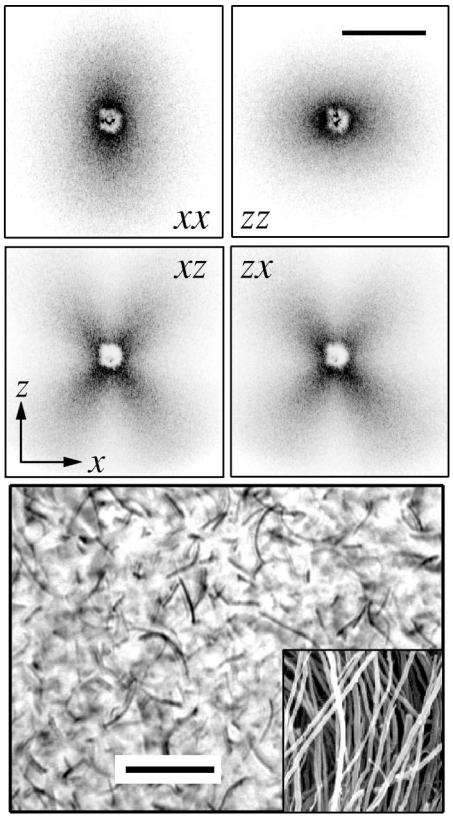

FIG. 5. Depolarized light-scattering patterns measured for an isotropic semidilute ($\phi \approx 3\times 10^{-3}$) MWNT-polymer suspension with a mean tube length and diameter comparable to those used in Fig. 4 ($L \approx 10\ \mu$m, $a \approx 25$ nm). The width of the upper right scale bar is 3.5 μm^{-1}. The lower image is a 200× optical micrograph of the same suspension, with a scanning electron microscopy image before dispersion as inset (width $=1.3\ \mu$m). The scale bar is 10 μm. Due to absorption, individual tubes appear as shadows on a bright incoherent background, in much the same way that incoherent light emitted on a dark background creates an image of a fluorescently labeled deoxyribose nucleic acid (DNA) molecule. As in the case of fluorescently labeled DNA, the MWNTs appear to be of larger diameter than they actually are.

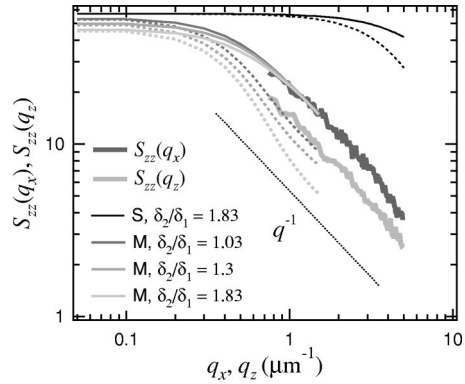

FIG. 6. The depolarized structure factor $S_{zz}(\mathbf{q})$ computed for varying anisotropy, where the dashed line shows q^{-1} power-law behavior. Scattering profiles have been generated for an isotropic distribution of $L=1\ \mu$m, $a=1$ nm SWNTs (upper curve) assuming $\delta_2/\delta_1 \approx 1.83$, and for isotropic distributions of $L=10\ \mu$m, $a=25$ nm MWNTs assuming $\delta_2/\delta_1 \approx 1.83$, 1.3, and 1.03, where the latter gives the best agreement with scattering data in Fig. 5.

ety of sources, including structural defects (in which case the deformation is "quenched" onto the tube), the flexure of extremely long suspended tubes due to thermal fluctuations in solution, and applied and residual hydrodynamic stresses acting on tubes in flowing suspensions and melts. The results derived in the previous sections can be generalized to include tube deformation *via* a renormalization of the dielectric anisotropy, $\alpha_\parallel$ and $\alpha_\perp$, and a generalization of the form amplitude, $f_l(\mathbf{q})$. As shown in Fig. 7, we can model the lth nanotube as N_l consecutive steps $\mathbf{r}_j\{l\}=b\hat{\mathbf{n}}_j\{l\}$, where b is the segment length and $L_l=bN_l$ is the contour length. The persistence length of the tube can then be defined as $\xi_p(l) \approx b[1-\langle \hat{\mathbf{n}}_j \cdot \hat{\mathbf{n}}_{j+1}\rangle_l]^{-1}$, where the brackets $\langle \ldots \rangle_l$ denote an internal conformational average over the lth nanotube. The local dielectric tensor of the jth element of this tube is given by Eq. (3):

$$(\alpha_\parallel-\alpha_\perp)\hat{\mathbf{n}}_j\hat{\mathbf{n}}_j+\alpha_\perp \mathbf{1}, \tag{46}$$

with the mean dielectric tensor of the tube given by

$$(\alpha_\parallel-\alpha_\perp)\langle \hat{\mathbf{n}}_j\hat{\mathbf{n}}_j\rangle_l+\alpha_\perp \mathbf{1}. \tag{47}$$

Using the decomposition

$$\langle \hat{\mathbf{n}}_j\hat{\mathbf{n}}_j\rangle_l=[\zeta_\parallel(l)-\zeta_\perp(l)]\hat{\mathbf{n}}_l\hat{\mathbf{n}}_l+\zeta_\perp(l)\mathbf{1}, \tag{48}$$

where the body director $\hat{\mathbf{n}}_l$ is the dominant eigenvector of $\langle \hat{\mathbf{n}}_j\hat{\mathbf{n}}_j\rangle_l$ with eigenvalue $\zeta_\parallel(l)$ and $\zeta_\perp(l)$ is the remaining

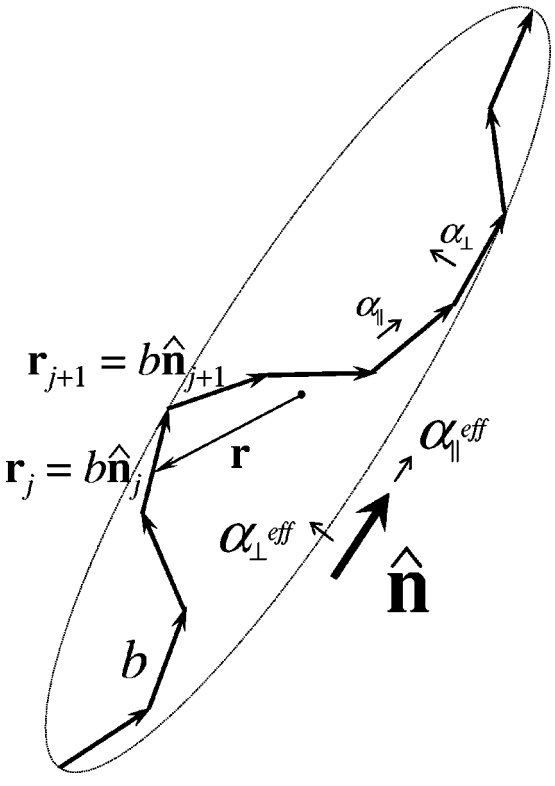

FIG. 7. To include deformation, we model a tube as the series of consecutive steps, $\mathbf{r}_j=b\hat{\mathbf{n}}_j$, where b is the segment length and $L=bN$ is the contour length. The body director, $\hat{\mathbf{n}}$, is the dominant eigenvector of the orientation tensor, $\langle \hat{\mathbf{n}}_j\hat{\mathbf{n}}_j\rangle$, and the moment tensor, $\langle \mathbf{rr}\rangle$, where the vector $\mathbf{r}$ locates an element of the tube with respect to its centroid. The eigenvalues of the former renormalize the optical anisotropy, while the eigenvalues of the latter define the ellipsoidal Gaussian envelope that gives a measure of the effective shape.

smaller (azimuthally-symmetric) eigenvalue, Eq. (47) becomes

$$(\alpha_\parallel-\alpha_\perp)[\zeta_\parallel(l)-\zeta_\perp(l)]\hat{\mathbf{n}}_l\hat{\mathbf{n}}_l+[\alpha_\perp+\zeta_\perp(l)(\alpha_\parallel-\alpha_\perp)]\mathbf{1}, \tag{49}$$

where $\mathrm{Tr}\langle\hat{\mathbf{n}}_j\hat{\mathbf{n}}_j\rangle=2\zeta_\perp+\zeta_\parallel=1$. Comparing Eq. (49) with the coarse-grained expression for the same quantity, $[\alpha_\parallel^{\mathrm{eff}}(l)-\alpha_\perp^{\mathrm{eff}}(l)]\hat{\mathbf{n}}_l\hat{\mathbf{n}}_l+\alpha_\perp^{\mathrm{eff}}(l)\mathbf{1}$, we obtain expressions for the renormalized anisotropy of the lth nanotube

$$\alpha_\perp^{\mathrm{eff}}(l)=\alpha_\perp+\zeta_\perp(l)(\alpha_\parallel-\alpha_\perp) \tag{50}$$

and

$$\alpha_\parallel^{\mathrm{eff}}(l)-\alpha_\perp^{\mathrm{eff}}(l)=(\alpha_\parallel-\alpha_\perp)[\zeta_\parallel(l)-\zeta_\perp(l)]. \tag{51}$$

The results of the preceding sections can be generalized *via* the substitutions $\alpha_\parallel\rightarrow\langle\alpha_\parallel^{\mathrm{eff}}(l)\rangle$ and $\alpha_\perp\rightarrow\langle\alpha_\perp^{\mathrm{eff}}(l)\rangle$, where the brackets denote an ensemble average over the suspension.

The second generalization involves the form amplitude, $f_l(\mathbf{q})$, as given by Eq. (21). Written out explicitly, this is

$$f_l(\mathbf{q})=\int_{v_l}d\mathbf{r}e^{-i\mathbf{q}\cdot\mathbf{r}}\approx\int_{v_l}d\mathbf{r}\left[1-i\mathbf{q}\cdot\mathbf{r}-\frac{1}{2}(\mathbf{q}\cdot\mathbf{r})^2+\ldots\right], \tag{52}$$

in the limit of small q. Integrating Eq. (52) term by term, the linear contribution vanishes, giving the Gaussian approximation

$$f_l(\mathbf{q})=v_l\left(1-\frac{1}{2}\mathbf{q}\cdot\langle\mathbf{rr}\rangle_l\cdot\mathbf{q}+\ldots\right)\approx v_l\exp\left(-\frac{1}{2}\mathbf{q}\cdot\langle\mathbf{rr}\rangle_l\cdot\mathbf{q}\right), \tag{53}$$

which depends on the moment tensor, $\langle\mathbf{rr}\rangle_l=v_l^{-1}\int_{v_l}d\mathbf{r}(\mathbf{rr})$. By symmetry, this will have the same principal axes as $\langle\hat{\mathbf{n}}_j\hat{\mathbf{n}}_j\rangle_l$, the dominant eigenvector being the body director, $\hat{\mathbf{n}}_l$. Denoting the large eigenvalue $(1/12)L_{\mathrm{eff}}^2(l)$ and the small eigenvalue $(1/4)a_{\mathrm{eff}}^2(l)$, a tube with its body director aligned with the x axis has

$$|f_l(\mathbf{q})|^2\approx v_l^2\exp[-\tfrac{1}{12}L_{\mathrm{eff}}^2(l)q_x^2-\tfrac{1}{4}a_{\mathrm{eff}}^2(l)q_\perp^2], \tag{54}$$

which when combined with Eqs. (27) and (28) is sufficient to include tube deformation in the Gaussian approximation, all of the previous results being generalized *via* the substitutions $L^2\rightarrow\langle L_{\mathrm{eff}}^2\rangle$ and $a^2\rightarrow\langle a_{\mathrm{eff}}^2\rangle$.

As a specific example we consider the Kratky–Porod model of a semiflexible chain with no torsional stress,[22] with the Hamiltonian

$$H=-\frac{\kappa}{b}\sum_{j=2}^{N}\hat{\mathbf{n}}_j\cdot\hat{\mathbf{n}}_{j-1}=-\frac{\kappa}{b}\sum_{j=2}^{N}\cos\theta_j, \tag{55}$$

where $\theta_j=\cos^{-1}(\hat{\mathbf{n}}_j\cdot\hat{\mathbf{n}}_{j+1})$ is the bending angle between successive orientation vectors, κ is the bending modulus, and the persistence length is $\xi_p=\kappa/k_BT$. The orientational correlation function decays exponentially with distance along the chain *via*[22]

$$\langle\hat{\mathbf{n}}_i\cdot\hat{\mathbf{n}}_j\rangle=e^{-b|i-j|/\xi_p}. \tag{56}$$

We assume that the chain is stiff, so that body director $\hat{\mathbf{n}}$ is approximately equivalent to $\mathbf{R}/R_g$, where

$$R_g^2=\langle\mathbf{R}^2\rangle=\left\langle\left(b\sum_{j=1}^{N}\hat{\mathbf{n}}_j\right)^2\right\rangle \tag{57}$$

is the mean-square end-to-end vector of the chain, which is simply related to the dominant eigenvalue of $\langle\mathbf{rr}\rangle$ defined earlier, and Eq. (57) can be evaluated in the limit of large N to obtain

$$R_g^2\approx\frac{Nb^2\sinh(b/\xi_p)}{\cosh(b/\xi_p)-1}\approx 2Nb\xi_p=2L\xi_p. \tag{58}$$

The remaining eigenvalue follows from the mean-square transverse displacement

$$R_\perp^2=N^{-1}\left\langle\sum_{j=1}^{N}[\mathbf{r}_{oj}-(\mathbf{r}_{oj}\cdot\hat{\mathbf{n}})\hat{\mathbf{n}}]^2\right\rangle, \tag{59}$$

where $\mathbf{r}_{oj}=b\Sigma_{i=1}^{j}\hat{\mathbf{n}}_i$ locates the jth segment of the tube with respect to one of its ends. For stiff chains in which the majority of segments lie on $\mathbf{R}$, this can be approximated by

$$R_\perp^2\approx b^2N^{-1}\sum_{j=2}^{N}\langle\theta_j^2\rangle=b^3/\xi_p, \tag{60}$$

where the second step follows from equipartition. Note that $R_\perp$ vanishes in the limit of large ξ_p, as expected. In a similar manner, it is straightforward to show that for $\langle\hat{\mathbf{n}}_j\hat{\mathbf{n}}_j\rangle$, $\zeta_\parallel\approx(2/N)(R_g/b)-1$ and $\zeta_\perp\approx1-(1/N)(R_g/b)$.

IX. CONCLUSIONS

We have derived an expression for the dielectric tensor of a dilute to semidilute suspension of optically anisotropic nanotubes. The result is expressed as a power series in the volume fraction, optical anisotropy, and optical contrast of the suspension. Within this framework, the connection to depolarized light scattering has been established and the results have been generalized to include tube deformation of arbitrary origin. A variety of rheo-optical data (light-scattering, optical microscopy, birefringence, and dichrosim) for flowing polymer-dispersed carbon nanotube suspensions will be analyzed elsewhere. By incorporating an independent measure of the shape of the tubes and the orientational distribution function, $p(\theta)$ (from stroboscopic video microscopy for MWNTs or small-angle neutron scattering for SWNTs, for example), we expect to obtain quantitative information about the optical anisotropy of carbon nanotubes that can then be used to quantify their orientation in flowing viscoelastic polymer melts. Although the results are derived in the dilute and semidilute limits, the results can be applied to more concentrated suspensions, for which $nL^3=(4/\pi)\phi_0(L/d)^2>1$ and $ndL^2=(4/\pi)\phi_0(L/d)>1$, by including interparticle correlations in a derivation of an effective form contribution that incorporates structure.[23]

We conclude by noting the paucity of optical anisotropy data on carbon nanotubes. In part, this reflects the scarcity of well-dispersed, well-aligned nanotube materials. For the sole purpose of measuring this anisotropy, elongational flows will yield better fiber alignment than shearing flows, and one could envision spinning composite fibers in noncrystalline polymer matrices that could then be optically probed at a variety of wavelengths to map out the full dielectric spec-

trum. All of the earlier results would directly apply to the analysis of such data. The formalism derived here might also prove useful in optical flow studies of any type of dilute or semidilute rod-like particle or fiber suspension, such as actin filaments, tobacco mosaic virus, worm-like micelles, and hematite rods,[24,25] in particular, which should also exhibit intrinsic absorption.

ACKNOWLEDGMENTS

The author thanks D. Fry and R. K. Hobbie for useful discussions, E. A. Grulke for providing the scanning electron microscopy image in Fig. 5, and H. Wang and H. Kim for assistance with the optical measurements and useful discussions.

[1] See, for example, G. G. Fuller, *Optical Rheometry of Complex Fluids* (Oxford University Press, New York, 1995), and references therein.
[2] M. Stoimenova, L. Labaki, and S. Stoylov, J. Colloid Interface Sci. **77**, 53 (1980).
[3] A. Peterlin and H. A. Stuart, Z. Phys. **112**, 1 (1939).
[4] See, for example, R. H. Baughman, A. A. Zakhidov, and W. A. de Heer, Science **297**, 787 (2002), and reference therein.
[5] E. K. Hobbie, H. Wang, H. Kim, C. Han, E. Grulke, and J. Obrzut, Rev. Sci. Instrum. **74**, 1244 (2003).
[6] A. Onuki and M. Doi, J. Chem. Phys. **85**, 1190 (1986).
[7] J. D. Jackson, *Classical Electrodynamics* (Wiley, New York, 1975).
[8] As a general rule, one must make the singularities explicit when evaluating integrals of Green's functions. Here, this is done *via* the substitution $\nabla^2 G(\mathbf{r}) = -\delta(\mathbf{r}) - k^2 G(\mathbf{r})$ and one must also exploit the fact that $\mathbf{E}_0 \cdot \mathbf{k} = 0$.
[9] We have used the relation $\delta(\mathbf{r}) = \lim_{\xi \to 0} (2\pi)^{-3/2} \xi^{-3} \exp(-r^2/2\xi^2)$ to obtain an expression for a correlation function of vanishing spatial extent and finite amplitude. This limit is only applicable if ξ goes to zero while the lower cutoff wavelength, Λ_0, is fixed, where the latter quantity sets the upper cutoff wave vector $q_c = 2\pi/\Lambda_0$. Physically, this corresponds to optically anisotropic particles too small to scatter light. The second term in Eq. (12) does not appear in the analysis of Onuki and Doi [A. Onuki and M. Doi, J. Chem. Phys. **85**, 1190 (1986)] because it is of higher order in products of the optical contrast, anisotropy, and volume fraction when there is segmental correlation, which will be quite strong for carbon nanotubes. We retain it here for a theoretical description that is rigorous to $O(\delta\tilde{\varepsilon}^2)$.
[10] The transformation from the notation used in E. K. Hobbie, H. Wang, H. Kim, C. Han, E. Grulke, and J. Obrzut [see Ref. 5] to that used here is made *via* the substitutions $\alpha_\parallel \to (\alpha_\parallel - \varepsilon_s)/\varepsilon_s$ and $\alpha_\perp \to (\alpha_\perp - \varepsilon_s)/\varepsilon_s$ in the previously derived expressions for the depolarized structure factors [Ref. 5]. In the present notation, the previously defined scattering parameters α and δ are $\alpha = [1/3(\alpha_\parallel + 2\alpha_\perp) - \varepsilon_s]/\varepsilon_s$ and $\delta = (\alpha_\parallel - \alpha_\perp)/\varepsilon_s$.
[11] N. J. Wagner, G. G. Fuller, and W. B. Russel, J. Chem. Phys. **89**, 1580 (1988).
[12] E. J. Hinch and L. G. Leal, J. Fluid Mech. **52**, 683 (1972).
[13] See, for example, E. K. Hobbie, H. Wang, H. Kim, S. Lin-Gibson, and E. A. Grulke, Phys. Fluids **15**, 1196 (2003), and references therein.
[14] C. A. Stover, D. L. Koch, and C. Cohen, J. Fluid Mech. **238**, 277 (1992).
[15] M. Rahnama, D. L. Koch, and E. S. G. Shaqfeh, Phys. Fluids **7**, 487 (1995).
[16] Y. Iso, D. L. Koch, and C. Cohen, J. Non-Newtonian Fluid Mech. **62**, 115 (1996).
[17] Y. Iso, C. Cohen, and D. L. Koch, J. Non-Newtonian Fluid Mech. **62**, 135 (1996).
[18] Deviations from the stress-optical rule have also been reported in branched polymer melts [S. B. Kharchenko and R. M. Kannan, Macromolecules **36**, 407 (2003)].
[19] T. A. J. Lenstra, Z. Dogic, and J. K. G. Dhont, J. Chem. Phys. **114**, 10151 (2001).
[20] Z. M. Li, Z. K. Tang, H. J. Liu, N. Wang, C. T. Chan, R. Saito, S. Okada, G. D. Li, J. S. Chen, N. Nagasawa, and S. Tsuda, Phys. Rev. Lett. **87**, 127401 (2001).
[21] Z. Yu and L. Brus, J. Phys. Chem. B **105**, 1123 (2001).
[22] See, for example, T. Strick, J. Allemand, V. Croquette, and D. Bensimon, Prog. Biophys. Mol. Biol. **74**, 115 (2000), and references therein.
[23] J. W. Bender and N. J. Wagner, J. Colloid Interface Sci. **172**, 171 (1995).
[24] S. J. Johnson and G. G. Fuller, J. Colloid Interface Sci. **124**, 441 (1988).
[25] S. J. Gason, D. V. Boger, and D. E. Dunstan, Langmuir **15**, 7446 (1999).